Journal of Catalysis 258 (2008) 345–355

Contents lists available at ScienceDirect

Journal of Catalysis

www.elsevier.com/locate/jcat

Oxidation of methanol to formaldehyde over a series of $Fe_{1-x}Al_x$-V-oxide catalysts

Robert Häggblad [a], Jakob B. Wagner [b], Staffan Hansen [b], Arne Andersson [a,*]

[a] Department of Chemical Engineering, Lund University, Chemical Center, P.O. Box 124, SE-221 00 Lund, Sweden
[b] Division of Polymer and Materials Chemistry, Department of Chemistry, Lund University, Chemical Center, PO Box 124, SE-221 00 Lund, Sweden

ARTICLE INFO

Article history:
Received 19 March 2008
Revised 26 June 2008
Accepted 27 June 2008
Available online 30 July 2008

Keywords:
Selective oxidation
Methanol
Formaldehyde
$Fe_{1-x}Al_xVO_4$ catalysts
Fe–V–O spinel-type phases
XRD
XANES
XPS
SEM
HRTEM

ABSTRACT

A series of triclinic $Fe_{1-x}Al_xVO_4$ phases with $0 \leqslant x \leqslant 1$ were prepared and used in the oxidation of methanol to formaldehyde. The activity measurements revealed that both the activity and especially the selectivity to formaldehyde increased with time of operation for at least 16 h, indicating restructuring of the catalysts. Characterisation of the catalysts with XRD, XANES, and electron microscopy after use in methanol oxidation showed that the stability of the bulk phases improved when Al was substituted for Fe in the structure. XRD and XANES of the used $FeVO_4$ showed that it partly transformed into a cation-vacant spinel-type $Fe_{1.5}V_{1.5}O_4$ phase, whereas the $AlVO_4$ phase showed no change in the bulk structure. HRTEM imaging of used catalysts confirmed that structural changes, including in the surface, occurred during catalysis. Quantitative surface analysis by XPS of the catalysts before and after use in methanol oxidation revealed no significant change in the metal composition, in good agreement with the corresponding bulk values, except for a lower Fe value. Steady-state activity data showed a modest increase in specific activity with the Al content, whereas the selectivity to formaldehyde was about 90% for all samples at high methanol conversion. The similar catalytic behaviour of the vanadates irrespective of the differences in the bulk structure indicates that the surface structure differed from the bulk structure. Compared with pure vanadia, the vanadates had lower activity per V atom and slightly greater selectivity to formaldehyde. Consequently, for methanol oxidation, the role of Al and Fe on the catalyst surface can be described as that of a spacer, decreasing the surface concentration of active V sites and the number of less selective V–O–V ensembles.

1. Introduction

Today, two competing processes, the silver and oxide processes, are used for the production of formaldehyde from methanol and air. The silver process uses a silver catalyst and operates with a methanol-rich feed (36–40%), whereas the oxide process uses an iron molybdate catalyst and a methanol-lean (~8.5%) feed. Which process is preferred is determined by the operating and capital costs, such as raw material and energy costs, as well as by plant size, product end use, and the type of operation [1–3].

Over the last decade, the oxide process has gained market share due to its higher selectivity to formaldehyde, around 93%. However, a major drawback of the present $MoO_3/Fe_2(MoO_4)_3$ catalyst is that it is deactivated as some of the molybdenum reacts with methanol to form volatile species at the reaction conditions, resulting in depletion of molybdenum from the catalyst in the reaction zone [4–8]. As a consequence, both the activity and the selectivity to formaldehyde decrease with time, and recondensation of the sublimed molybdenum in colder regions causes an increased pressure drop [7], necessitating replacing the catalyst after 1–2 years of operation [4]. Consequently, alternative Mo-free catalysts are of interest [9], but only on the condition that the alternatives are almost as selective as the iron molybdate catalyst at high methanol conversion, because methanol makes the largest contribution to the production cost.

In the area of alternative catalysts for methanol oxidation, several studies have been reported on vanadia-based catalysts including pure vanadia, mixed oxides, and supported vanadia [10–13]. In particular, vanadates with Ni, Fe, Co, Mg, Cr, Mn, Al, Ag, Cu, and Zn have been found to have selectivities >90% to formaldehyde at high methanol conversion [9,14–17]. According to Wachs et al. [16], the vanadium in bulk metal vanadates is not volatile in methanol oxidation, although XPS analysis before and after use of the samples in methanol oxidation indicated some structural changes in the surface and near surface layers during catalysis. Besides the surface structure, such changes may involve the formation of new phases; in oxidation catalysis on bulk metal oxides, not only the surface, but also the catalyst bulk structure may change under the influence of the catalytic reaction until steady state is reached [18]. Consequently, in the present work, we investigated in more detail the performance and the stability of a $Fe_{1-x}Al_xVO_4$ series of catalysts with x varying from 0 to 1. The catalysts were characterised

* Corresponding author.
E-mail address: arne.andersson@chemeng.lth.se (A. Andersson).

0021-9517/$ – see front matter
doi:10.1016/j.jcat.2008.06.029

Table 1
Notation, specific surface area and phase composition of prepared catalysts

Catalyst notation	Specific surface area (m^2/g)	Phase composition
Fe_1Al_0	15.2	Triclinic $(Fe_1Al_0)VO_4$
$Fe_{0.75}Al_{0.25}$	13.2	Triclinic $(Fe_{0.75}Al_{0.25})VO_4$
$Fe_{0.50}Al_{0.50}$	22.1	Triclinic $(Fe_{0.50}Al_{0.50})VO_4$
$Fe_{0.25}Al_{0.75}$	9.3	Triclinic $(Fe_{0.25}Al_{0.75})VO_4$
Fe_0Al_1	10.8	Triclinic $(Fe_0Al_1)VO_4$

by XRD, XANES, XPS, SEM, and HRTEM both before and after use in methanol oxidation to produce formaldehyde.

2. Experimental

2.1. Catalyst preparation

$Fe_{1-x}Al_xVO_4$ catalysts with $x = 0, 0.25, 0.50, 0.75$, and 1 were prepared by precipitation from a homogeneous water solution containing dissolved V and Fe and/or Al. The homogeneous solution was prepared from two separate water solutions, a 0.04 M NH_4VO_3 (Merck) solution and a 0.5 M solution of $Fe(NO_3)_3{\cdot}9H_2O$ (Merck) and/or $Al(NO_3)_3{\cdot}9H_2O$ (Sigma–Aldrich). The two well-stirred solutions were mixed together and homogenised by lowering the pH to 1.0 by adding 3 M HNO_3. A solid precipitate then was obtained when the pH was rapidly raised to 4.0 by the addition of 3 M NH_3. Particle coarsening was carried out to stimulate particle recovery [19] by heating the turbid solution for 2 h at 50 °C under stirring. The particles were separated by centrifugation (3000 rpm for 3 min) and then washed three times with water, acetone, and water. Finally, the samples were dried for 16 h at 80 °C and then calcined for 6 h at 580–620 °C depending on the phase purity. Table 1 summarises the notation, specific surface area, and phase composition of the catalysts.

2.2. Activity measurements

The prepared catalysts were tested for methanol oxidation to produce formaldehyde in a stainless steel reactor operating at isothermal conditions and atmospheric pressure. To obtain isothermal conditions, the reactor was embedded in an aluminium block placed in a tube furnace. For the measurements, the catalyst sample was ground into fine powder and pressed into tablets, which were then crushed and sieved to particles of 0.250–0.425 mm diameter. The reactor was loaded with the desired amount of catalyst diluted three times with quartz particles. The catalyst was heated up to the reaction temperature in a flow of 10 ml/min O_2 and 84 ml/min N_2. When the reaction temperature 350 °C was reached, a gaseous methanol flow of 6 ml/min was added to the flow of oxygen and nitrogen. The product flow composition was analysed every 20 min for 1 h and then once an hour for the next 15 h.

Methanol, formaldehyde (FA), dimethyl ether (DME), methyl formate (MF), dimethoxymethane (DMM), and CO_2 were analysed with an online gas chromatograph equipped with a Haysep C column and both flame ionisation and thermal conductivity detectors. CO was analysed online with a Rosemount Binos 100 IR analyser.

2.3. Catalyst characterisation

The specific surface areas of the catalysts were measured with a Micromeritics Flowsorb 2300 instrument. The single-point BET method was used with nitrogen adsorption at liquid nitrogen temperature and subsequent desorption at room temperature. All samples were degassed at 150 °C for 24 h before analysis.

Powder X-ray diffraction (XRD) analysis was performed on a Seifert XRD 3000 TT diffractometer using Ni-filtered Cu Kα radiation and a rotating sample holder. Data were collected between 5 and 80 degrees 2θ in steps of 0.1° (2.0 s/step). The unit cell parameters of the five $Fe_{1-x}Al_xVO_4$ catalysts were determined both before and after the catalysts' use in methanol oxidation. Crystal structure data were taken from Ref. [20] for $FeVO_4$, from Ref. [21] for $AlVO_4$, and from Ref. [22] for the spinel-type structure observed in the used Al-free sample.

XPS analysis was performed on a PHI 5500 XPS instrument using monochromatic Al Kα radiation. Powder samples were placed on a conducting and sticky tape. To minimise the effects of sample charging, the aluminium-containing samples were charge-neutralised by electrons. PC-ACCESS and MuliPak 6.1A software were used to evaluate the data, and the quantifications were made using a Shirley function for the background. The C 1s peak was used as an energy reference and was set to a binding energy of 285.0 eV. Data used for quantification of the element were collected using a sufficient amount of sample to exclude any signal from the underlying carbon film. However, due to the charge accumulation observed for the Al-containing preparations, resulting in peak broadening and asymmetry, the data used to determine the valence states by peak fitting had to be collected separately using a small amount of very well-ground sample placed on a conducting film. In addition, the sample was continuously neutralised with electrons to compensate for the electrons ejected during the measurements. Because the oxidation number of Al is surely trivalent, the charge compensation was adjusted to give symmetric Al 2p and Al 2s peaks, indicating that no charge effects were present. Using this technique, analysis on the $Fe_{0.50}Al_{0.50}$ sample was carried out without peak broadening and asymmetry. For the Fe_0Al_1 sample, the charge accumulation problem was too extensive to give reliable data, however.

The XANES measurements were performed at the I811 beamline at Maxlab (Lund University) using a Si(111) double-crystal monochromator and three ionisation chambers. Spectra of the Fe K- and V K-edges were recorded in transmission mode using Fe and V metal foils as energy references. The sample was placed in between the first and the second ionisation chambers, and the reference was placed before the third chamber. To obtain an optimal absorption signal, the sample was diluted with boron nitride.

Scanning electron microscopy (SEM) images were acquired with a Jeol 6700F FEG SEM. The acceleration voltage was set to 5 kV; the working distance, to 7 mm. For high-resolution transmission electron microscopy (HRTEM) imaging, the samples were studied in a Jeol 3000F FEG TEM operated at 300 kV. EELS was performed using an attached Gatan GIF2002 image filter. The samples were dry-dispersed on standard Cu grids with holey carbon films for TEM inspection.

3. Results

3.1. Catalytic behaviour

The catalytic performance of the pure triclinic $Fe_{1-x}Al_xVO_4$ phases listed in Table 1 was evaluated for methanol oxidation. Fig. 1 shows the methanol conversion and selectivity to formaldehyde given as a function of time on stream for the Fe_1Al_0, $Fe_{0.50}Al_{0.50}$, and Fe_0Al_1 catalysts. The degree of conversion was high, with a between-sample variation of 95–98%. After 16 h on stream, in all three preparations, the difference between the initial and the final value of the methanol conversion was small; however, a noticeable increase in the selectivity to formaldehyde with time could be seen. All three preparations had similar features: a rapid initial increase in selectivity, followed by an asymptotic feature reaching a selectivity of 88–91% after 16 h on stream.

Fig. 2 presents activity and selectivity data for the five prepared $Fe_{1-x}Al_xVO_4$ catalysts. All catalysts showed rather similar activity, with a trend toward activity increasing up to about a factor

of two when Fe was replaced with Al. The product selectivities shown in Fig. 2 are for high methanol conversion (95–98%). For formaldehyde, the selectivity was about 88–91% and the differences among the samples were small. For the main byproducts CO_x and DME, the selectivities were in the ranges 9–12% and 0.3–1.6%, respectively. No significant differences among the catalysts were detected. Two possible weak trends were increasing selectivity to DME but decreasing selectivity to CO_x with increasing Al content. Compared with the corresponding data shown in Fig. 2 for a commercial-type $MoO_3/Fe_2(MoO_4)_3$ catalyst, the vanadates were more active but slightly less selective to formaldehyde and DME, because they produced more carbon oxides. But compared with the data for pure vanadia, the vanadates were less active and somewhat more selective for formaldehyde formation. On the pure vanadia, in contrast to the other samples, a small amount of methyl formate also was formed.

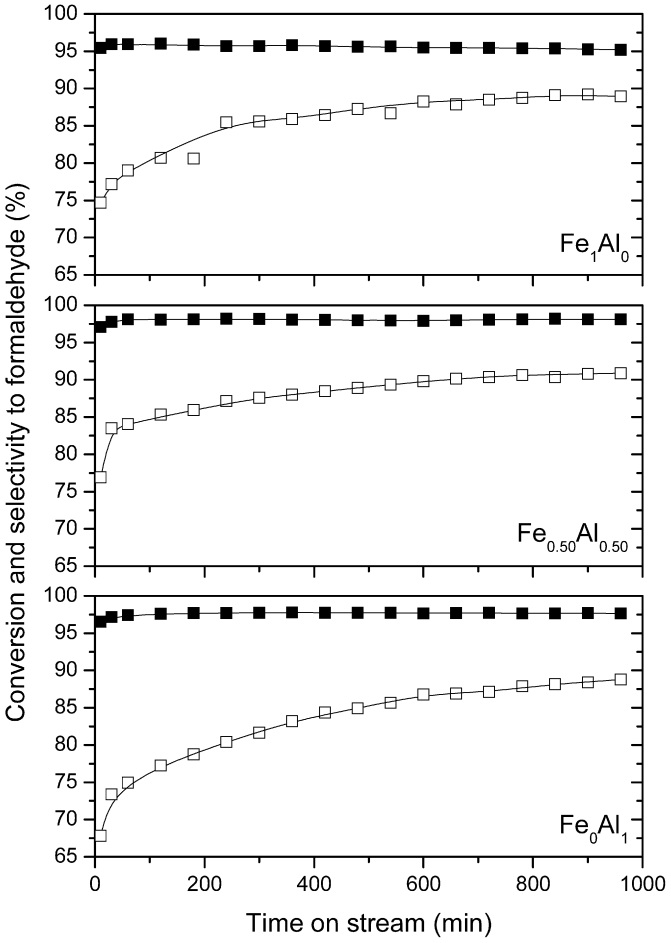

Fig. 1. Methanol conversion (■) and selectivity to formaldehyde (□) as measured for the Fe_1Al_0, $Fe_{0.50}Al_{0.50}$ and Fe_0Al_1 catalysts as a function of time on stream at 350 °C and high methanol conversion (>95%). The inlet gas composition is 6 vol% methanol and 10 vol% oxygen in nitrogen.

3.2. X-ray diffraction

The catalyst were characterised by XRD both as synthesised and after use in methanol oxidation, with the samples designated fresh and used, respectively. The XRD patterns of the freshly prepared samples are displayed in Fig. 3. All samples show the characteristic features of a triclinic ($P-1$) type of phase, isostructural with $FeVO_4$ [20,23] and $AlVO_4$ [21,24]. The lattice parameters of the pure $Fe_{1-x}Al_xVO_4$ phases were refined; the values obtained are given in Table 2. The *a*-, *b*-, and *c*-axes all show a linear dependence with the degree of substitution, confirming the successful preparation of a solid solution series of $Fe_{1-x}Al_xVO_4$ catalysts.

The XRD patterns of the used samples are displayed in Fig. 4. Comparing this figure with Fig. 3 clearly shows that the used Fe_1Al_0 consists of the original triclinic $FeVO_4$ phase to only a slight extent. Instead, a new diffraction pattern is notable, with broad and intense peaks at 30.4, 35.5, 43.7, 57.7, and 63.1 degrees 2θ. As the subtraction diffractogram in Fig. 5 shows, the new phase formed is a spinel-type phase, similar to Fe_3O_4 (magnetite) and γ-Fe_2O_3 (maghemite). The six strongest diffraction peaks are at 30.2, 35.6, 43.1, 53.5, 57.1, and 62.6 degrees 2θ for Fe_3O_4 and at 30.3, 35.8, 43.4, 53.9, 57.4 and 63.0 degrees 2θ for γ-Fe_2O_3. The broadness of the peaks for the used Fe_1Al_0 indicates that the crystallites were small in the spinel-type phase formed during catalysis.

For the used $Fe_{0.50}Al_{0.50}$ and Fe_0Al_1 catalysts, the diffraction patterns in Fig. 4 do not reveal the appearance of any new peaks

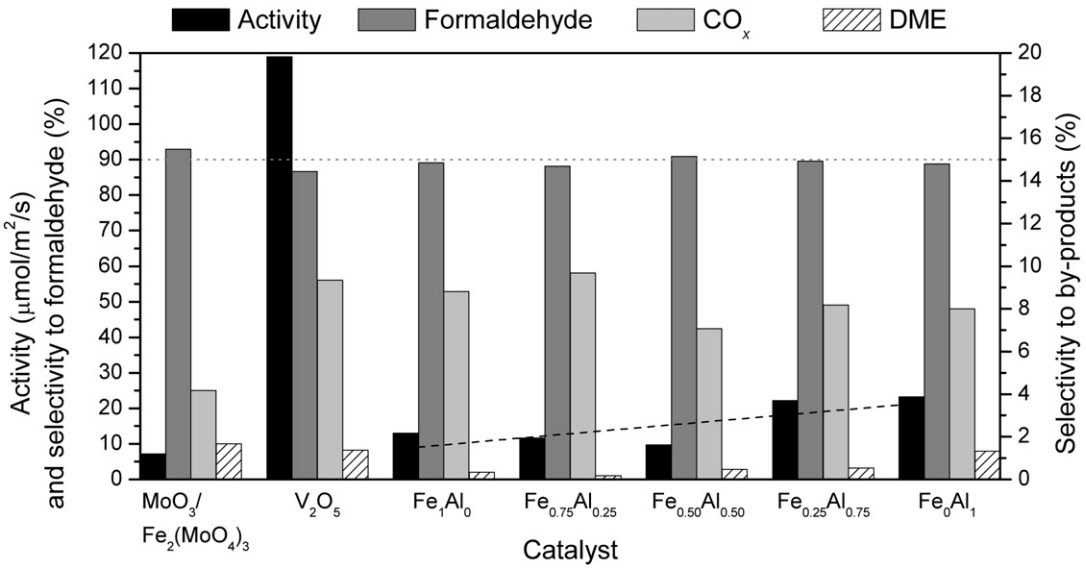

Fig. 2. Catalytic data as measured after 16 h on stream at 350 °C for a series of $Fe_{1-x}Al_xVO_4$ catalysts with $x = 0, 0.25, 0.50, 0.75$ and 1. Corresponding data for a commercial type $MoO_3/Fe_2(MoO_4)$ catalyst and pure vanadia are included for comparison. For obtaining the specific activities measurements were made at low methanol conversion, admitting calculation of the specific rates for the defined inlet gas composition. The selectivities to formaldehyde, CO_x and dimethyl ether (DME) are for high methanol conversions in the range 95–99%, which is the region of interest in full scale production. Inlet gas composition: 6 vol% methanol and 10 vol% oxygen in nitrogen.

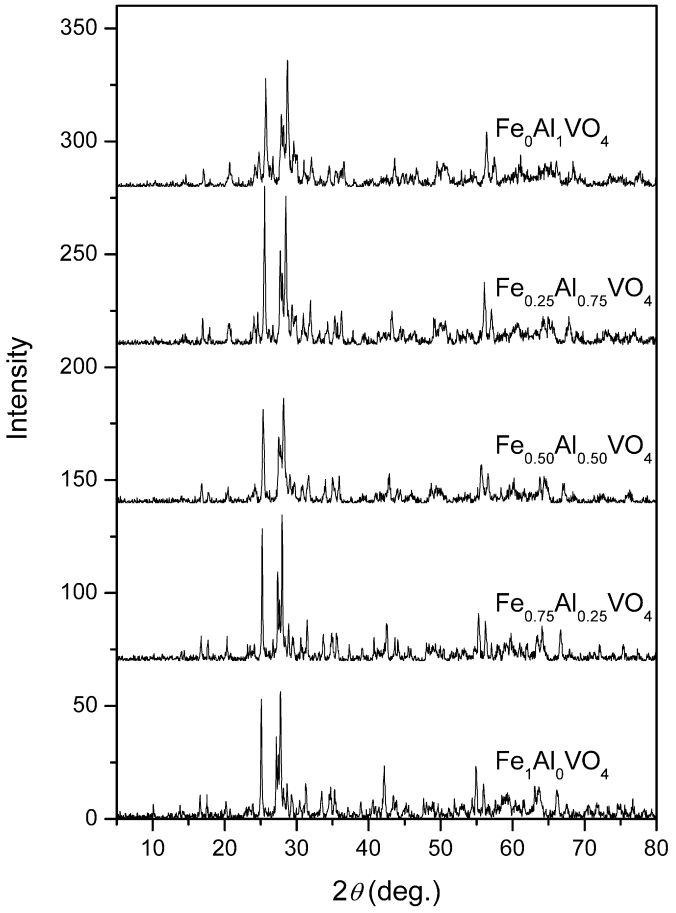

Fig. 3. XRD patterns of freshly prepared $Fe_{1-x}Al_xVO_4$ catalysts, showing a series of isostructural phases from $FeVO_4$ to $AlVO_4$.

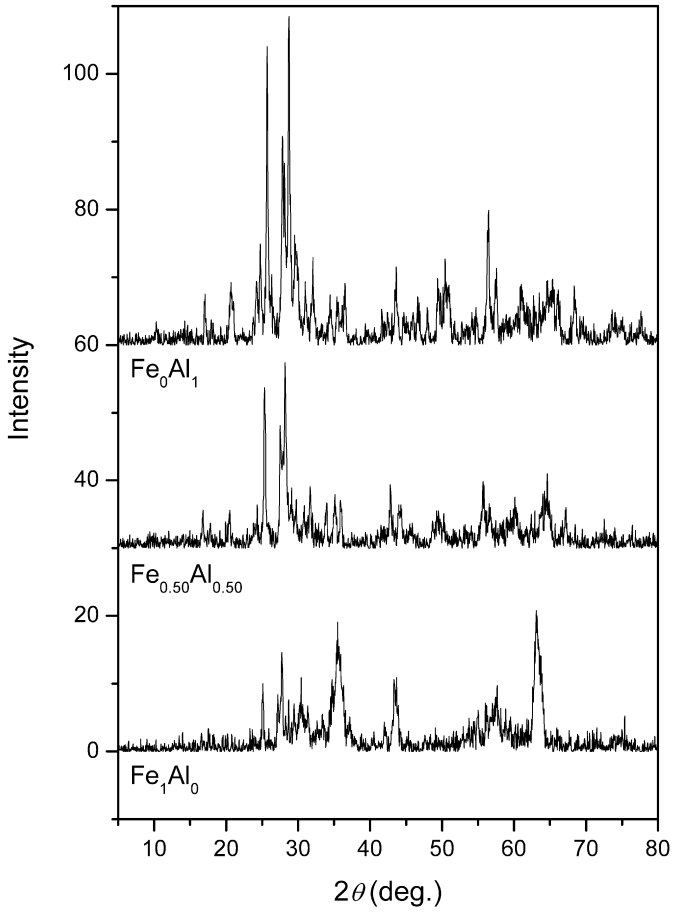

Fig. 4. XRD patterns for the Fe_1Al_0, $Fe_{0.50}Al_{0.50}$ and Fe_0Al_1 catalysts recorded after use of the samples for 16 h in methanol oxidation. A comparison with Fig. 3 reveals that the used Fe_1Al_0 sample contains only a small amount of the original phase, and relatively more of the original phase is preserved when increasing the Al content in the catalyst.

Table 2
Refined unit cell parameters for the triclinic $Fe_{1-x}Al_xVO_4$ phases in fresh and used catalysts

Samples[a]	a (Å)	b (Å)	c (Å)	α (°)	β (°)	γ (°)
Fresh catalysts						
Fe_1Al_0	6.708	8.051	9.334	96.7	106.6	101.5
$Fe_{0.75}Al_{0.25}$	6.664	7.985	9.291	96.5	106.7	101.5
$Fe_{0.50}Al_{0.50}$	6.631	7.929	9.259	96.4	106.9	101.4
$Fe_{0.25}Al_{0.75}$	6.576	7.829	9.192	96.3	107.0	101.4
Fe_0Al_1	6.536	7.758	9.129	96.2	107.3	101.4
Used catalysts						
Fe_1Al_0	Unit cell parameters resemble those of the fresh sample[b]					
$Fe_{0.75}Al_{0.25}$	ND[c]					
$Fe_{0.50}Al_{0.50}$	6.62	7.924	9.234	96.4	106.8	101.4
$Fe_{0.25}Al_{0.75}$	ND[c]					
Fe_0Al_1	6.537	7.756	9.128	96.2	107.3	101.4

[a] For notations, see Table 1.
[b] The sample consisted of mainly a cubic spinel phase with $a = 8.33$ Å.
[c] Not determined.

compared with the patterns of the corresponding fresh samples shown in Fig. 3. This finding is confirmed by the subtraction patterns shown in Fig. 5.

3.3. XANES

To determine the valences of the bulk elements, XANES measurements were performed on the fresh and used Fe_1Al_0, $Fe_{0.50}Al_{0.50}$, and Fe_0Al_1 catalysts. Fig. 6 shows the V K-edge spectra of the catalysts. The main edge position for the fresh Fe_1Al_0, $Fe_{0.50}Al_{0.50}$, and Fe_0Al_1 was 5481.5 eV for all preparations, whereas the positions were 5477.4, 5481.0, and 5481.3 eV, respectively, for the corresponding used catalysts. Thus, the energy shifts between the fresh and the used Fe_1Al_0, $Fe_{0.50}Al_{0.50}$, and Fe_0Al_1 were −4.1, −0.5 and −0.2 eV, respectively, indicating reduction of vanadium in the bulk. Moreover, the magnitude of the shift shows that the degree of reduction decreased with increasing Al content in the catalyst.

The Fe K-edge spectra of fresh and used Fe_1Al_0 and $Fe_{0.50}Al_{0.50}$ catalysts are displayed in Fig. 7a. The edge positions for the fresh Fe_1Al_0 and $Fe_{0.50}Al_{0.50}$ samples were 7127.7 and 7127.6 eV, respectively. For the used catalysts, the corresponding positions shifted toward lower energy and appeared at 7124.9 and 7127.1 eV, respectively. According to the XRD patterns shown in Figs. 4 and 5, the major phase in the used Fe_1Al_0 is of spinel-type similar to both Fe_3O_4 and γ-Fe_2O_3. Fig. 7b compares the Fe K-edge spectra for the used Fe_1Al_0 catalyst with those for Fe_3O_4 and γ-Fe_2O_3. It shows that the edge position for the used Fe_1Al_0 was very close to that for γ-Fe_2O_3 with Fe^{3+} only, whereas the edge for Fe_3O_4 with both Fe^{2+} and Fe^{3+} was further shifted toward lower energy. This finding indicates that Fe can be trivalent in the bulk of the used Fe_1Al_0 and $Fe_{0.50}Al_{0.50}$ catalysts. Consequently, the shift in edge position between the fresh and the used catalysts (Fig. 7a) apparently does not have to be due to reduction of Fe, but rather to differences in the coordination of Fe.

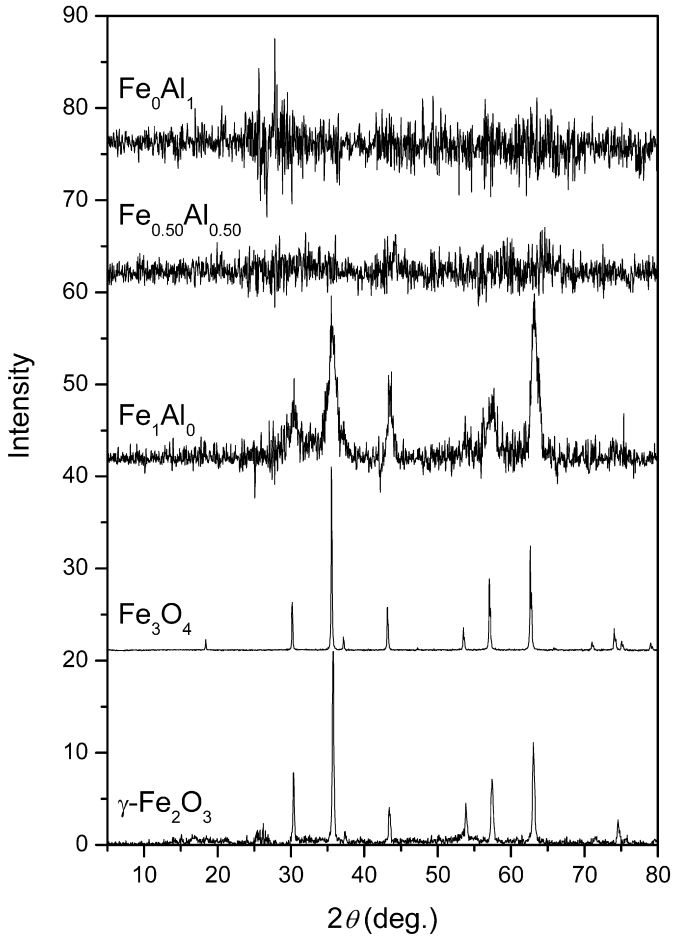

Fig. 5. XRD subtraction patterns for the used Fe_1Al_0, $Fe_{0.50}Al_{0.50}$ and Fe_0Al_1 catalysts obtained by subtracting the patterns of the fresh catalysts (Fig. 3) from the corresponding patterns of the used catalysts (Fig. 5). The diffractograms of the spinel-type phases Fe_3O_4 and γ-Fe_2O_3 are shown for comparison.

3.4. XPS

XPS measurements were performed to determine the elemental composition and the oxidation states of the elements in the surface region. The surface compositions of fresh and used Fe_1Al_0, $Fe_{0.50}Al_{0.50}$, and Fe_0Al_1 are given in Table 3. No significant difference in the surface compositions can be observed between fresh and used catalysts. The data show that the concentration of V at the surface varies from 14.1 to 19.3%, which values are similar to the value of 16.7% for the bulk. Iron, on the other hand, is significantly underrepresented at the surface, whereas Al shows similar values as the bulk.

The Al 2s, Fe $2p_{3/2}$, and V $2p_{3/2}$ binding energies for fresh and used catalysts are given in Table 4. The data show that the binding energy for Al 2s was practically the same for fresh and used samples, about 119.4 eV. This value is the same as that reported for Al_2O_3 [25], demonstrating the presence of Al^{3+} in the catalysts in all cases. In addition, the measured Fe $2p_{3/2}$ binding energy values were approximately the same for the fresh and used preparations of Fe_1Al_0 and $Fe_{0.50}Al_{0.50}$, varying between 711.3 and 711.6 eV. The values agree with those reported for $FeVO_4$ [26], Fe_2O_3 [26,27], and FeOOH [27], verifying that Fe at the surface of the present catalysts is trivalent. In all cases, a symmetric Fe $2p_{3/2}$ peak was observed, revealing no other oxidation state for Fe than Fe^{3+}.

Opposed to the Al 2s and Fe $2p_{3/2}$ peaks, the V $2p_{3/2}$ peaks for the used samples were not always symmetric, indicating the presence of more than one oxidation state. Table 5 gives the binding energy, peak width (FWHM), and relative amounts of the different oxidation states of V as determined by resolution of the V $2p_{3/2}$ peaks for fresh and used Fe_1Al_0 and $Fe_{0.50}Al_{0.50}$ shown in

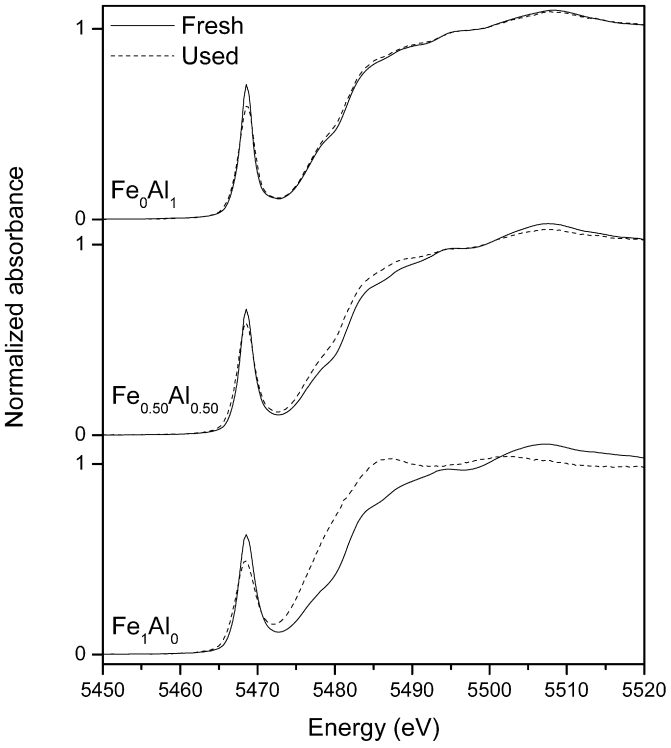

Fig. 6. Normalised V K-edge XANES spectra for fresh and used Fe_1Al_0, $Fe_{0.50}Al_{0.50}$ and Fe_0Al_1 catalysts.

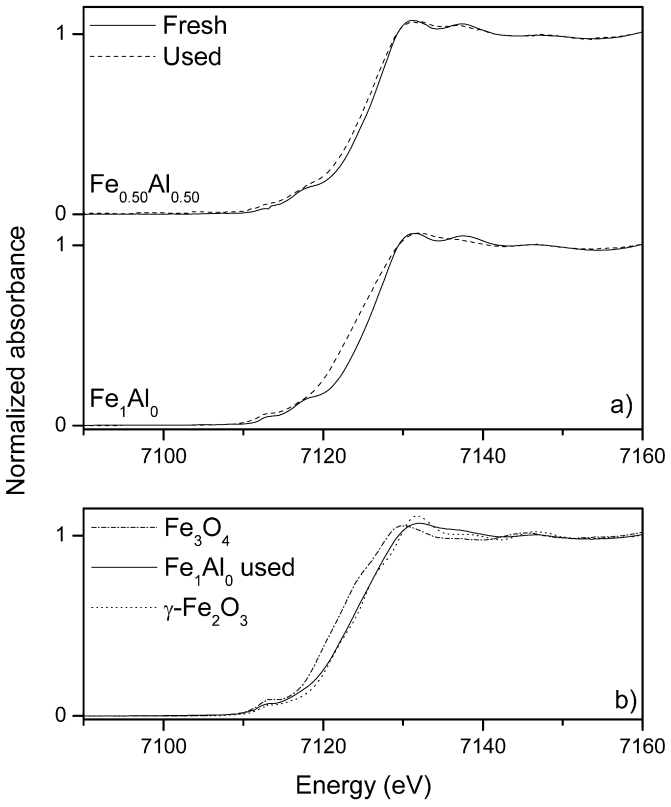

Fig. 7. Normalised Fe K-edge XANES spectra for (a) the fresh and the used Fe_1Al_0 and $Fe_{0.50}Al_{0.50}$ catalysts, and (b) Fe_3O_4, γ-Fe_2O_3 and the used Fe_1Al_0 catalyst.

Table 3
Bulk compositions of the catalysts and the surface compositions as determined by XPS

Catalyst	Bulk composition (at%)				XPS fresh catalyst (at%)				XPS used catalyst (at%)			
	V	Fe	Al	O	V	Fe	Al	O	V	Fe	Al	O
Fe_1Al_0	16.7	16.7	0	66.7	18.6	12.2	–	69.2	19.3	9.5	–	71.2
$Fe_{0.50}Al_{0.50}$	16.7	8.3	8.3	66.7	16.8	5.6	10	67.7	15.8	5.2	10.2	68.8
Fe_0Al_1	16.7	0	16.7	66.7	14.1	–	16.2	69.7	15.7	–	16.5	67.8

Table 4
Catalyst binding energies determined by XPS

Catalyst	Binding energy of fresh catalyst (eV)				Binding energy of used catalyst (eV)			
	Fe $2p_{3/2}$	O 1s	V $2p_{3/2}$	Al 2s	Fe $2p_{3/2}$	O 1s	V $2p_{3/2}$	Al 2s
Fe_1Al_0	711.3	530.4	517.2	–	711.5	530.6	517.5	–
$Fe_{0.50}Al_{0.50}$	711.6	530.7	517.7	119.4	711.6	530.6	517.5	119.5
Fe_0Al_1	–	530.3	517.2	119.6	–	530.9	517.8	119.2

Table 5
Data for vanadium in the catalysts as obtained after resolution of the V $2p_{3/2}$ peak into its components by peak fitting

Sample	V^{5+}			V^{4+}			V^{3+}		
	FWHM (eV)	BE[a] (eV)	V^{5+}/V_{tot} (%)	FWHM (eV)	BE[a] (eV)	V^{4+}/V_{tot} (%)	FWHM (eV)	BE[a] (eV)	V^{3+}/V_{tot} (%)
Fresh catalysts									
Fe_1Al_0	1.12	517.2	100.0						
$Fe_{0.50}Al_{0.50}$	1.20	517.7	100.0						
Used catalysts									
Fe_1Al_0	1.15	517.6	70.7	1.20	516.5	24.5	1.20	515.2	4.7
$Fe_{0.50}Al_{0.50}$	1.30	517.5	90.9	1.30	516.3	9.1			

[a] BE: binding energy.

Fig. 8. No data are given for higher Al content, because in this case the analysis was strongly affected by charging effects. For the fresh samples, the spectra in Fig. 8 show symmetric V $2p_{3/2}$ peaks with a binding energy of about 517.4 eV (Table 5), which can be assigned to V^{5+} [28,29]. The fact that the peaks are symmetric indicates the presence of only one oxidation state. The V $2p_{3/2}$ spectra for the samples used in methanol oxidation show a shoulder from reduced V on the low-energy side of the peak maximum. The shoulder is more pronounced in the spectrum of the used Fe_1Al_0 than in that for the used $Fe_{0.50}Al_{0.50}$. Peak fitting was performed as shown in Fig. 8. The V $2p_{3/2}$ peak of the used Fe_1Al_0 can be resolved into the three components, V^{5+} (517.6 eV), V^{4+} (516.5 eV), and V^{3+} (515.2 eV) [28,29], whereas the spectrum for the used $Fe_{0.50}Al_{0.50}$ shows only two oxidation states, V^{5+} (517.5 eV) and V^{4+} (516.3 eV). The quantitative data given in Table 5 indicate more severe reduction of Fe_1Al_0 (~70% V^{5+}) than of $Fe_{0.50}Al_{0.50}$ (~90% V^{5+}) after use in methanol oxidation.

3.5. SEM

Fig. 9 presents characteristic SEM images of fresh and used Fe_1Al_0 samples. The fresh Fe_1Al_0 sample consisted of approximately 100 nm large and well-separated spherical particles (Fig. 9a). Although XRD findings demonstrated bulk transformation of the sample (Figs. 4 and 5), the SEM images of the sample after catalytic testing revealed the same overall structure of 100-nm spherical particles (Fig. 9b).

Compared with the Al-free sample, the fresh $Fe_{0.50}Al_{0.50}$ sample had slightly larger (~150 nm) and less distinct particles, whereas the fresh Fe_0Al_1 sample consisted of particles agglomerated into a less porous substance. The corresponding used samples were very similar to the respective fresh samples, but the used $Fe_{0.50}Al_{0.50}$ had slightly smaller particles.

3.6. TEM

In general, the samples were very sensitive to the electrons in the TEM. To avoid beam damage, the electron dose was minimised, so that the samples were not altered during image acquisition. Fig. 10a shows a high-resolution image of the fresh Fe_1Al_0 sample. The 100-nm particles consisted of $FeVO_4$ single crystals embedded in a 5- to 10-nm-thick layer showing lattice fringes, indicating that the layer was crystalline. Because of the low electron dose used, it was not possible to obtain reliable quantitative analytical data from the crystalline shell. Qualitatively, however, EELS analyses showed that both the core crystal and shell structure consisted of iron, vanadium, and oxygen. After catalytic testing, according to SEM, the Fe_1Al_0 sample had the same overall morphology as the fresh sample (see Figs. 9a and 9b). Fig. 10b presents a TEM image of a corner of a 100-nm particle, showing that the particle comprised smaller 5–10 nm crystalline particles and most likely voids, somewhat connected in a crystalline matrix, as indicated by the lattice fringes. EELS of the V $L_{2,3}$ and Fe $L_{2,3}$ ionisation edges revealed a shift toward lower energy loss compared with the fresh catalyst, in agreement with the corresponding XANES spectra shown in Figs. 6 and 7.

The HRTEM images of the Fe_0Al_1 samples in Fig. 11 show 10- to 50-nm crystals in the form of large agglomerates. The smaller crystal size compared with the iron-containing samples gives the sample a smoother, less porous appearance. Fig. 11a shows the crystals of the fresh sample embedded in a thin (1 nm), apparently amorphous layer. After catalytic testing, the sample had a thicker (2–4 nm), amorphous layer (Fig. 11b). Furthermore, both the fresh and the used catalysts had 5-nm crystals at the surface of the larger crystals. It was not possible to determine the exact composition of the small particles, because of the low EELS signal. Elemental mapping by means of energy-filtered TEM showed homogeneous vanadium and iron signals; however, the lack of spatial resolution because of the low signal intensity made it difficult to reliably distinguish the 5-nm crystals in the elemental map.

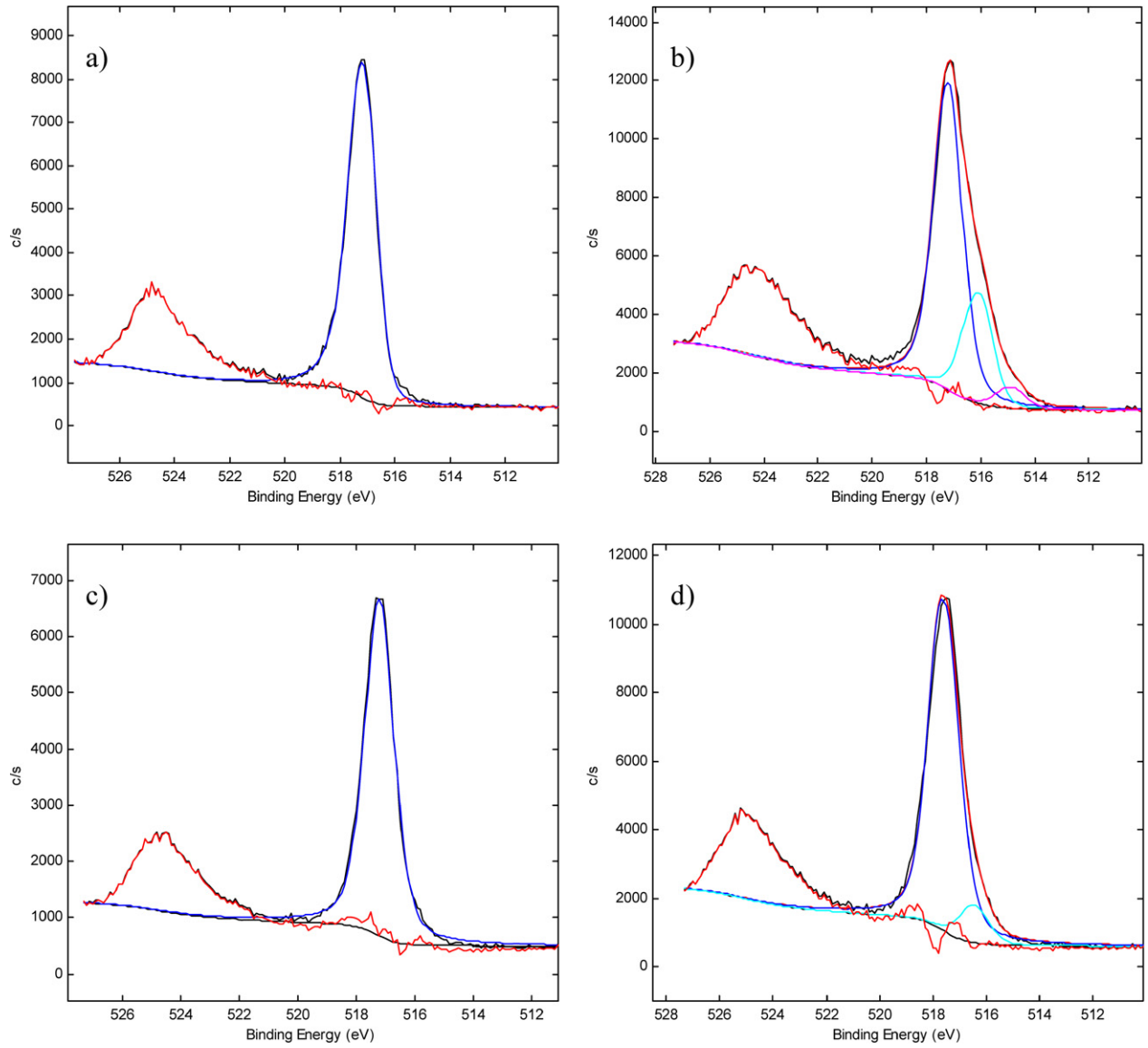

Fig. 8. XPS spectra of the V 2p region for (a) fresh Fe_1Al_0, (b) used Fe_1Al_0, (c) fresh $Fe_{0.50}Al_{0.50}$, and (d) used $Fe_{0.50}Al_{0.50}$, showing for the V $2p_{3/2}$ peak also the contributions of different oxidation states as obtained by peak fitting.

Compared with Fe_0Al_1, the $Fe_{0.50}Al_{0.50}$ sample showed similar features on HRTEM, with small (5–10 nm) crystalline particles at the surface of larger (150 nm) single crystal particles, although the particles were more distinct and less agglomerated.

4. Discussion

4.1. Bulk phases

The XRD patterns shown in Fig. 3 and the variations of the unit cell data given in Table 2 definitely confirm the successful preparation of a $Fe_{1-x}Al_xVO_4$ series of triclinic phases from $FeVO_4$ to $AlVO_4$. In the structure with V in tetrahedral coordination, the valences of the cations were V^{5+}, Fe^{3+}, and Al^{3+} [20,21,23,24], in agreement with our XANES spectra given in Figs. 6 and 7 showing the V and Fe K-edges for the fresh catalysts. The graph in Fig. 12, showing the V K-edge positions for a number of compounds with vanadium in different oxidation state and coordination [30] together with the data for our fresh and used catalysts, confirms the presence of V^{5+} in the fresh catalysts.

The catalytic data in Fig. 1 show changes in the activity and especially the selectivity to formaldehyde extending over several hours of operation, clearly indicating that structural transformation of the catalyst bulk and/or surface occurred in methanol oxidation. Comparing the XRD patterns for the freshly prepared Fe_1Al_0 in Fig. 3 with those for the used catalyst in Figs. 4 and 5 shows that a partial transformation of the bulk occurred from the triclinic-type $FeVO_4$ structure in the fresh sample to a spinel-type structure in the used sample. Although SEM revealed no changes in either particle size or morphology (Fig. 9), imaging of the catalyst by HRTEM confirmed a major change in the bulk structure due to its use in methanol oxidation (Fig. 10). Elemental mapping in HRTEM showed that the new phase formed, of a spinel type and similar in structure to Fe_3O_4 and γ-Fe_2O_3 (Fig. 5), contained not only iron, but also vanadium. Such types of spinels have been prepared previously [31–37]. The structural formula for $V_xFe_{3-x}O_4$ spinels with $0 \leqslant x \leqslant 2$ has been expressed in more detail as $(Fe^{2+}_{\alpha}Fe^{3+}_{1-\alpha})_A(Fe^{2+}_{1-\alpha}Fe^{3+}_{1-\alpha}V^{3+}_{x})_BO^{2-}_4$ with $\alpha = x/2$ and tetrahedral (A) and octahedral (B) sites [33]. Thermal studies of this type of spinel phase have demonstrated that oxidation of Fe^{2+} and V^{3+} to form Fe^{3+} and V^{5+} via V^{4+} is possible with preservation

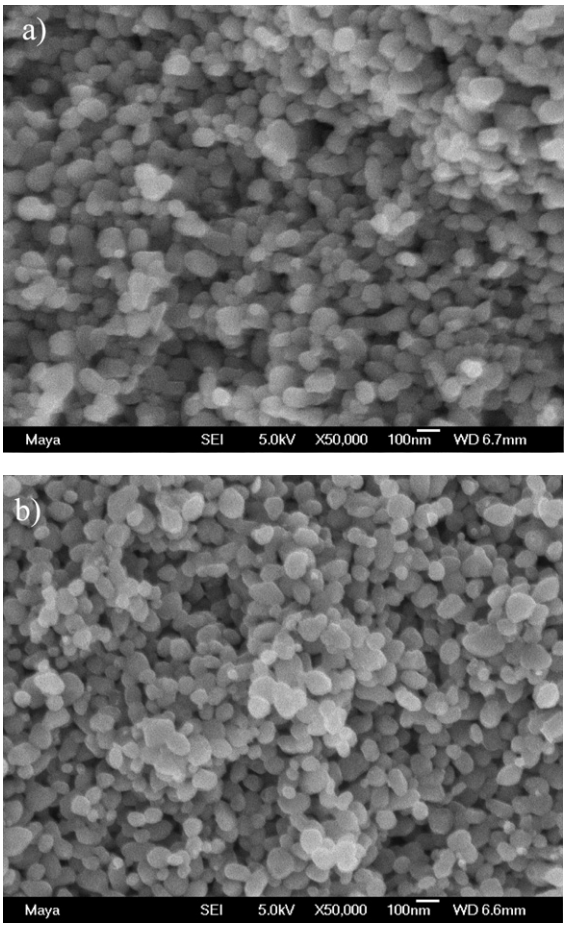

Fig. 9. SEM images of (a) fresh Fe_1Al_0 and (b) used Fe_1Al_0.

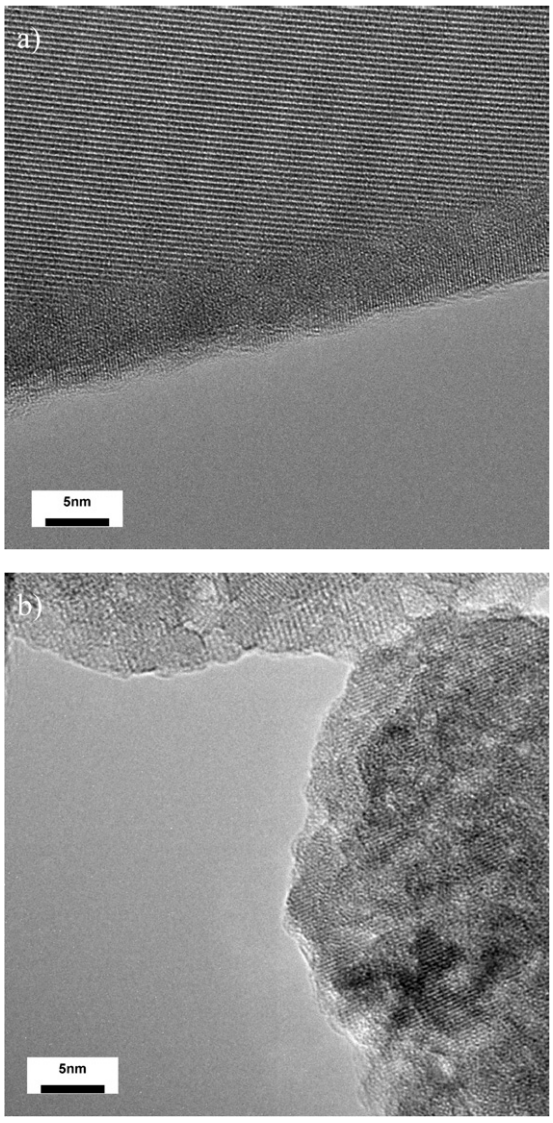

Fig. 10. HRTEM images of the Fe_1Al_0 catalyst (a) before and (b) after use in methanol oxidation for 16 h.

of the basic spinel-type structure [33,34,36,38]. The oxidation of the cations was accompanied by the appearance of a corresponding number of cation vacancies in the structure to maintain the electroneutrality.

The V K-edge XANES spectrum for the used Fe_1Al_0 in Fig. 6 shows a shift of about 4 eV toward lower energy compared with that for the fresh sample. According to the correlation shown in Fig. 12, a shift of this magnitude corresponds to an average valence of +3.9 for V in this sample. Because the used Fe_1Al_0 catalyst consists of both the triclinic $FeVO_4$ phase and a spinel-type phase, subtracting the contribution from the triclinic phase to the XANES spectrum would be possible if the phase composition of the sample were known. Then, from the edge position in the resulting spectrum, it would be possible to determine the oxidation state for the vanadium in the spinel structure. An estimate of the content of the triclinic phase in the used Fe_1Al_0 sample can be obtained by comparing the diffractogram of the used sample with that of the phase pure fresh sample with regard to some typical XRD peaks from the triclinic phase. Using the intensities of the two strongest peaks from the triclinic phase (25.0° and 27.8° 2θ) for the comparison, the calculated intensity ratios, $I_{\text{used}}/I_{\text{fresh}}$, indicate that about 20–25% of triclinic $FeVO_4$ was present in the used Fe_1Al_0 catalyst. From this value, the V K-edge position of the spinel phase (E_{Spinel}) can be estimated, assuming that the measured edge position ($E_{\text{Experimental}}$) is equal to the sum of the contributions from the two constituent phases according to $E_{\text{Experimental}} = y_{\text{Triclinic}} \cdot E_{\text{Triclinic}} + (1 - y_{\text{Triclinic}}) \cdot E_{\text{Spinel}}$, where $y_{\text{Triclinic}}$ is the estimated content of $FeVO_4$ and $E_{\text{Triclinic}}$ is the edge position as measured for the fresh sample consisting of the pure $FeVO_4$. According to the graph in Fig. 12, the value of 5476.2 eV calculated for E_{Spinel} corresponds to an average V valence of +3.5. Using the same approach for the Fe K-edge spectra, from the estimated edge position for the spinel-type phase, an average Fe valence of +2.84 is obtained by interpolating between the edge positions for Fe_3O_4 and γ-Fe_2O_3 with an average Fe valence of +2.67 and +3, respectively.

For a $V_xFe_{3-x}O_4$ spinel with $x = 1.5$, corresponding to the atomic ratio V/Fe = 1 in Fe_1Al_0, a stoichiometric phase without any vacancies can be formulated as $V(III)_{1.5}Fe(II)_{1.0}Fe(III)_{0.5}O_4$. Considering the average valences determined for V and Fe in the used Fe_1Al_0 sample, the composition of the oxidised spinel phase in this sample will be $V(III)_{0.63}V(IV)_{0.63}Fe(II)_{0.20}Fe(III)_{1.06}\square_{0.48}O_4$, where □ denotes a cation vacancy. It has been found that the vacancies can be located at both octahedral and tetrahedral sites in the spinel-type structure, whereas the reduced V are in octahedral positions [34]. The latter finding agrees with the fact that the intensity of the V K-pre-edge peak is lower in the XANES spectrum of the used Fe_1Al_0 than in the spectrum for the fresh sample (Fig. 6), considering that the intensity of the pre-edge peak for V is expected to decrease with increasing symmetry from tetrahedral to octahedral coordination [30].

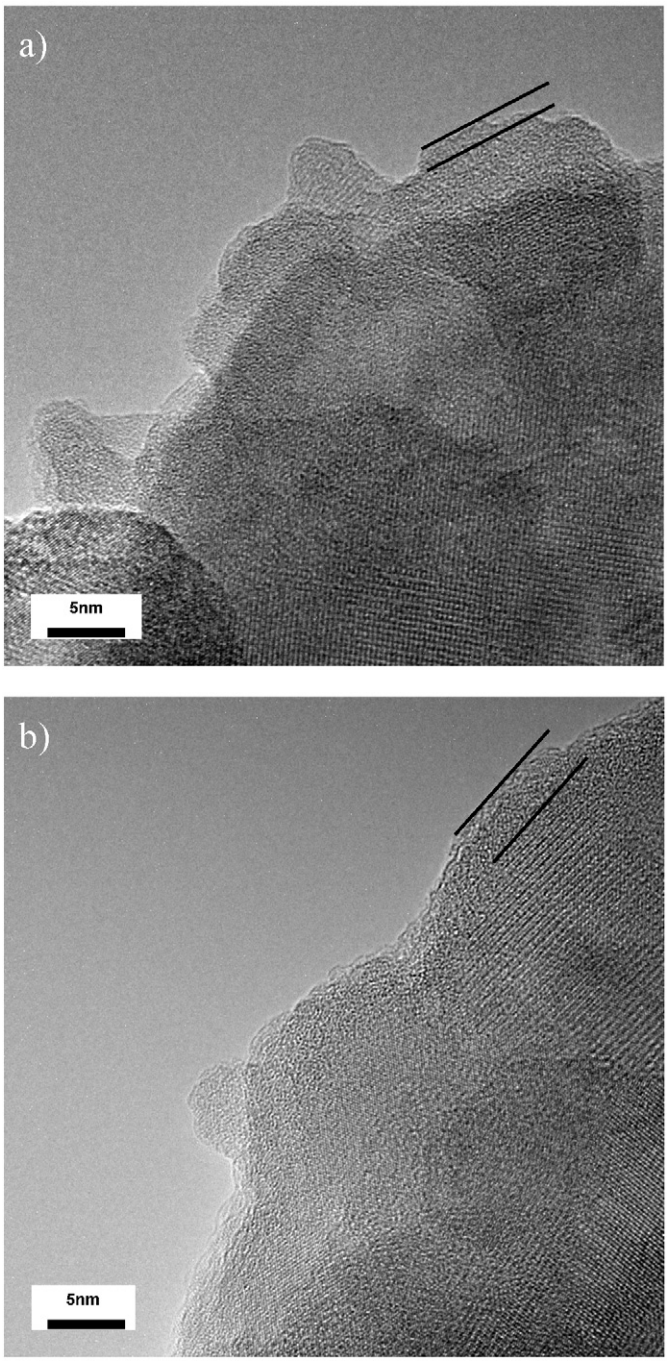

Fig. 11. HRTEM images of the Fe_0Al_1 catalyst (a) before and (b) after use in methanol oxidation for 16 h. An apparently amorphous surface layer, which has become thicker after use of the sample in methanol oxidation, is indicated in the figure.

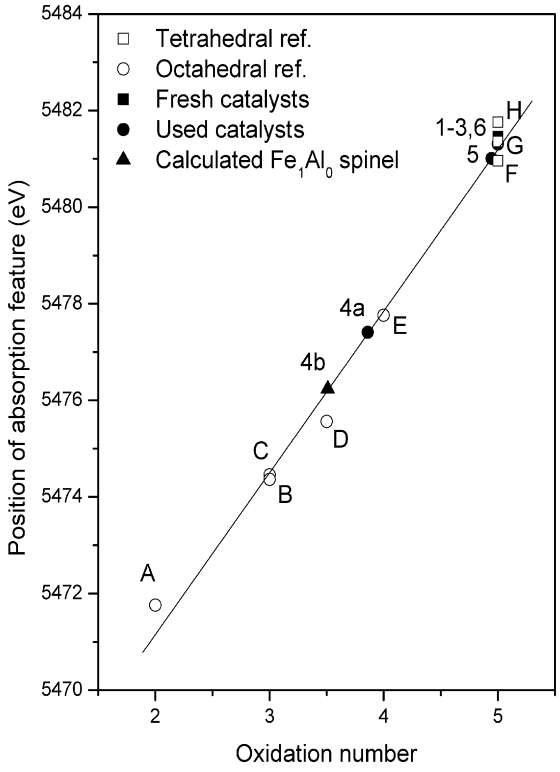

Fig. 12. The V K-edge positions for fresh and used $Fe_{1-x}Al_xVO_4$ catalysts and reference compounds with V in various type of coordination. Freshly prepared (1) Fe_1Al_0, (2) $Fe_{0.50}Al_{0.50}$ and (3) Fe_0Al_1; and the corresponding used catalysts (4a) Fe_1Al_0, (4b) Fe_1Al_0 after subtraction of the contribution of the triclinic phase, (5) $Fe_{0.50}Al_{0.50}$ and (6) Fe_0Al_1 being submitted to methanol oxidation for 16 hours. Data for the reference compounds are from Ref. [27] and are marked (A) VO, (B) $KAlV_2Si_3O_{10}(OH)_2$, (C) V_2O_3, (D) V_4O_7, (E) V_2O_4, (F) NH_4VO_3, (G) $CrVO_4$ and (H) $Pb_5(VO_4)_3Cl$, where vanadium is tetrahedrally coordinated in A–E and octrahedrally in F–H.

Regarding the used $Fe_{0.50}Al_{0.50}$ catalyst, the data for the unit cell axes in Table 2 indicate that the triclinic phase in this sample is richer in Al compared with the fresh sample. The unit cell has become slightly smaller, in agreement with Al^{3+} being a smaller cation than Fe^{3+} [39]. From the variations of the unit cell axes in Table 2, the composition of the triclinic phase in the used $Fe_{0.50}Al_{0.50}$ is estimated to be approximately $Fe_{0.48}Al_{0.52}VO_4$, indicating the concurrent formation of either $FeVO_4$, a spinel-type $V_xFe_{3-x}O_4$ phase, or vanadium and iron oxides. From the stoichiometry of the Al-rich triclinic phase, it follows that the total amount of the minor phase or phases can be only about 3 wt%. Usually such a small amount cannot be detected on XRD; the XRD patterns of the used $Fe_{0.50}Al_{0.50}$ in Figs. 4 and 5 show peaks only from the triclinic phase. Moreover, HRTEM revealed no formation of new structures, although the SEM images showed that the particles in the catalyst were slightly smaller after the catalyst was used in methanol oxidation. That some structural changes in the catalyst occurred during methanol oxidation is verified by the minor shift in the position of the V K-edge (Fig. 6), the magnitude of which, according to the correlation shown in Fig. 12, indicates an average valence of +4.9 for the V in the used $Fe_{0.50}Al_{0.50}$ catalyst. In parallel, some shift in the Fe K-edge position also occurred, as shown in Fig. 7. Together, these findings suggest that a small amount of a spinel-type $V_{1.5}Fe_{1.5}O_4$ was formed during catalysis.

The data for the fresh and the used Fe_0Al_1 catalyst in Table 2 show the same unit cell dimensions for both samples, indicating that no bulk transformation of the triclinic $AlVO_4$ phase occurred from its use methanol oxidation. Further support for the stability of the $AlVO_4$ bulk in methanol oxidation is provided by the XRD patterns for the used Fe_0Al_1 in Figs. 4 and 5, the XANES spectra in Fig. 6, and the relationship illustrated in Fig. 12, showing exclusively V^{5+} in the used sample. But the HRTEM images in Fig. 11 reveal some changes at the surfaces, with the thickness of the apparently amorphous surface layer increasing from 1 nm in the fresh catalyst up to 2–4 nm in the used catalyst.

4.2. Surface composition and catalytic performance

Despite the observation that depending on the Al content, the $Fe_{1-x}Al_xV$-oxide series of catalysts exhibited widely varying degrees of bulk transformation after use in methanol oxidation, all of the samples exhibited very similar activation behaviour during the

first 16 h on stream, as shown in Fig. 1. That observation clearly indicates that the surface structure, which determines the catalytic properties, changes over time until steady state is reached. Indeed, Wachs et al. [40] observed similar changes with time of the catalytic performance in methanol oxidation starting from physical mixtures of V_2O_5 and TiO_2 or MoO_3 and TiO_2. Using in situ Raman characterisation, the investigators showed that reaction-induced spreading of vanadia and molybdena occurs, forming 2-dimensional overlayers on the support. Moreover, experimental results have been reported suggesting that the surface of bulk metal vanadates [16] and molybdates [41–43] may consist only of surface vanadium oxide and molybdenum oxide species, respectively. Considering the fact that there is little variation in activity and selectivity between the $Fe_{1-x}Al_xV$-oxide samples (Fig. 2), it can be proposed that the activation behaviour is due to reaction-induced surface enrichment of vanadium from the bulk. But the quantitative XPS data in Table 3 give no support for the activation being primarily related to enrichment of vanadium at the surface. Although the V/Fe ratio for Fe_1Al_0 increased from 1.5 to 2.0, the V/(Fe + Al) atomic ratios for $Fe_{0.50}Al_{0.50}$ and Fe_0Al_1 were almost the same before and after the catalysts were used in methanol oxidation. For $Fe_{0.50}Al_{0.50}$, the ratio changed from 1.1 to 1.0 and for Fe_0Al_1, the ratio was 0.9 both before and after use; that is, both samples showed V/(Fe + Al) ratios very close to the value of 1.0 for the bulk. This indicates that the observed activation behaviour is due to adjustment of the surface structure under the influence of the reactants. In catalysis, the surface structure is determined not only by the bulk structure to which it is attached, but also by the surface interacting with the components being adsorbed from the gas phase, the reaction conditions, and the associated kinetic parameters [18]. Moreover, the finding of an activation period of at least 16 h suggests that the restructuring involves not only the true surface, but also possibly a few layers beneath. Some support for this suggestion is given by the HRTEM images of the bulk stable iron-free Fe_0Al_1 catalyst in Fig. 11, showing a thicker, apparently amorphous layer in the sample used in methanol oxidation compared with the fresh sample.

The modest increase with the Al content of the activity per surface area unit (Fig. 2) definitely was not due to any parallel increase at the surface of the V concentration, which, according to the XPS results, was higher for Fe_1Al_0 than for the Al-containing samples (Table 3). Rather, the variation in activity with the catalyst composition can be related to differences induced by the bonding of V to either Fe or Al in the form of V–O–Fe or V–O–Al, respectively. XPS demonstrated a reduction of V in the samples used in methanol oxidation, as shown in Table 5 and Fig. 8. Moreover, the degree of reduction diminished with increasing Al content of the catalyst, in line with the observed reduction of the bulk. Therefore, the possibility that the reduction detected by XPS may be from a few layers beneath the surface and that the vanadium in the true surface layer may be predominately pentavalent irrespective of the bulk composition of the catalyst cannot be excluded, considering that the catalyst activities were of similar magnitude and, moreover, that reoxidation usually is not considered rate-limiting in methanol oxidation [44,45]. Concerning the differences between the catalysts with regard to the bulk reduction behaviour, it should be noted that the reduction of the bulk is an initial transient process not necessarily indicating any major difference in the reoxidation rate of the catalyst surfaces under steady-state conditions.

For supported oxide systems, Wachs et al. [46,47] reported that the turnover frequency for methanol oxidation decreased with increasing electronegativity of the metal cation of an oxide support, suggesting that the electron density on the bridging oxygen in the V–O–support bond, or, alternatively, the electron density on the vanadium atom [48], determines the turnover frequency. Assuming a monolayer of metal oxide with approximately 12 μmol cations/m^2 surface area, with half of the cations on the vanadates being vanadium, the activities per V atom calculated from the data given in Fig. 2 were 9.9, 3.9, and 2.2 mol methanol/(mol V s) for pure vanadia, Fe_0Al_1, and Fe_1Al_0, respectively. The finding that the activities per V atom decreased in the same order as the Sanderson electronegativity values increased, V (1.39) > Al (1.71) > Fe (2.20), in line with previous findings [46,47], can be attributed to the electron density on the bridging oxygen decreasing in the order V–O–V > V–O–Al > V–O–Fe. A greater electron density should facilitate abstraction of the hydrogen atom from the slightly acidic hydroxyl group of methanol, thereby increasing the surface concentration of intermediate methoxy species. But the adsorption of methanol in the form of a methoxy species is known to be an easy step [42,46], and the methoxy species can even be mobile at the surface [49], whereas the abstraction of hydrogen from the adsorbed methoxy species is rate-limiting [44,50]. In fact, experimental results have indicated that increasing the electron density at the active site improves the rate constant even more than the adsorption constant [45].

Although there is general consensus in the literature and spectroscopic evidence for the formation of $V–OCH_3$ species [45,46,48], there is still some disagreement about the details of the final hydrogen abstraction. Weckhuysen and Keller [48] have proposed that a high electron density on the vanadium facilitates breaking of the C–H bond, giving formaldehyde and an intermediate V–H bond. According to recent theoretical calculations [51,52], hydrogen abstraction from the methoxy group may involve H transfer to a vanadyl oxygen atom; however, the literature gives experimental evidence that a bridging oxygen rather than a vanadyl oxygen determines the activity [12,48].

The finding that the selectivity to formaldehyde did not vary much among the vanadate samples and was around 90% for all of the samples at high methanol conversion is in agreement with data previously reported for $FeVO_4$ and $AlVO_4$ [9,16]. Our observation that pure vanadia gave somewhat lower selectivity (87%) is in agreement with previous results [53]. Consequently, for methanol oxidation, the role of Fe and Al in the vanadates can be described as that of a "spacer," creating isolation of the V sites and thereby decreasing the number of V–O–V sites. As the data in Fig. 2 indicate, compared with the V–O–Fe and V–O–Al sites, the V–O–V sites gave slightly more DME and carbon oxides, respectively. Comparing the product distributions obtained in methanol oxidation on bulk metal vanadates and other metal oxides suggests that the metal vanadates contain only surface vanadium sites [16]. Concerning our $Fe_{1-x}Al_xV$-oxide series of catalysts, neither the quantitative XPS data in Table 3 nor the activities expressed per V atom give support for significantly enriching the surfaces with vanadium. The selectivity data for the vanadates in Fig. 2 show that the selectivity to formaldehyde was practically the same irrespective of whether the second cation was Fe or Al, demonstrating that these elements are rather inert in the surface structure. Although iron oxide produces predominately carbon dioxide from methanol, it has very low activity as expressed per surface area unit [43,54]. Moreover, our comparative measurements on a low-surface area α-alumina (Norpro, 5 m^2/g, XPS Na/Al ratio = 0.05) showed that it was inactive for methanol, in contrast to high-surface area γ-alumina producing DME [12]. The trend shown in Fig. 2 toward increasing selectivity to DME with increasing Al content of the vanadate agree with the finding of acidic Al sites producing DME from methanol present on the surface. However, a DME selectivity of <2% for Fe_0Al_1 confirms that the Al on the Fe(Al)–V–O catalysts contributes little to the selectivity.

5. Conclusion

Our findings indicate that catalysts prepared in the form of phase pure triclinic $Fe_{1-x}Al_xVO_4$ phases with $0 \leqslant x \leqslant 1$ were active and selective for methanol oxidation to produce formaldehyde. When submitted to methanol oxidation, all of the triclinic phases initially showed very similar activation behaviour extending for at least 16 h of operation. During this period, both the conversion and especially the selectivity to formaldehyde increased with time on stream. The extended behaviour indicates restructuring of the surface and the near-surface region to form a surface structure different from that of the bulk. Supporting information provided by HRTEM imaging showed growth of an apparently amorphous layer at the surface of the bulk stable $AlVO_4$.

Elemental analysis by XPS showed no significant difference in the metal composition between the freshly prepared samples and the corresponding samples used in methanol oxidation. Moreover, except for some depletion of Fe, the V/(Fe + Al) atomic ratios determined by XPS agreed quite well with the corresponding bulk ratios.

Compared with an industrial type $MoO_3/Fe_2(MoO_4)_3$ catalyst, the vanadates were more active per unit surface area and less selective to formaldehyde at high methanol conversion (∼90% vs 93%). Compared with pure vanadia, the vanadates were less active per vanadium atom and per unit surface area, but more selective to formaldehyde (∼90% vs 87%). Substituting Al for Fe gave slightly improved activity but had no notable effect on the selectivity to formaldehyde. The activity data indicate that the electron density on a bridging V–O–M (M = V, Al, Fe) oxygen determined the activity, with increasing activity expressed per V atom decreasing the electronegativity of the M metal. The improved selectivity to formaldehyde of the vanadates compared with pure vanadia suggests that the Al and Fe in the structure create isolation of V and decrease the number of less-selective V–O–V sites.

XRD and XANES showed that the triclinic $FeVO_4$ phase was unstable under the reaction conditions and formed a cationvacant spinel-type $Fe_{1.5}V_{1.5}O_4$ phase. Substituting Al for Fe in the catalyst gave more stable bulk structures.

Acknowledgments

The Swedish Research Council (VR) is acknowledged for financial support.

References

[1] G. Reuss, W. Disteldorf, A.O. Gamer, A. Hilt, in: Ullmann's Encyclopedia of Industrial Chemistry, vol. A11, seventh ed., Wiley–VCH, Weinheim, 2008, pp. 619–652.
[2] B. Crichton in: Informally Speaking (Newsletter from Perstorp Formox, http://www.perstorpformox.com), spring/summer 2003, pp. 12–13.
[3] A.R. Chauvel, P.R. Courty, R. Maux, C. Petitpas, Hydrocarbon Process. 52 (9) (1973) 179.
[4] A. Andersson, M. Hernelind, O. Augustsson, Catal. Today 112 (2006) 40.
[5] A.P.V. Soares, M.F. Portela, A. Kiennemann, J.M.M. Millet, React. Kinet. Catal. Lett. 75 (2002) 13.
[6] A.P.V. Soares, M.F. Portela, A. Kiennemann, L. Hilaire, Chem. Eng. Sci. 58 (2003) 1315.
[7] N. Burriesci, F. Garbassi, M. Petrera, G. Petrini, N. Pernicone, in: B. Delmon, G.F. Froment (Eds.), Catalyst Deactivation, Elsevier, Amsterdam, 1980, pp. 115–126.
[8] B.I. Popov, V.N. Bibin, G.K. Boreskov, Kinet. Katal. (Eng. Transl.) 17 (1976) 322.
[9] I.E. Wachs, L.E. Briand, US Patent 7 193 117 B2, 2007, to Lehigh University.
[10] P. Forzatti, E. Tronconi, A.S. Elmi, G. Busca, Appl. Catal. A 157 (1997) 387.
[11] T. Kim, I.E. Wachs, J. Catal. 255 (2008) 197.
[12] G. Deo, I.E. Wachs, J. Catal. 146 (1994) 323.
[13] S. Lim, G.L. Haller, Appl. Catal. A 188 (1999) 277.
[14] R. Maliński, React. Kinet. Catal. Lett. 5 (1976) 265.
[15] R. Maliński, M. Akimoto, E. Echigoya, J. Catal. 44 (1976) 101.
[16] L.E. Briand, J.-M. Jehng, L. Cornaglia, A.M. Hirt, I.E. Wachs, Catal. Today 78 (2003) 257.
[17] G.V. Isaguliants, I.P. Belomestnykh, Catal. Today 100 (2005) 441.
[18] A. Bielański, J. Haber, Oxygen in Catalysis, Dekker, New York, 1991.
[19] S. Denis, E. Baudrin, M. Touboul, J.-M. Tarascon, J. Electrochem. Soc. 144 (1997) 4099.
[20] B. Robertson, E. Kostiner, J. Solid State Chem. 4 (1972) 29.
[21] E. Arisi, S.A. Palomares Sánchez, F. Leccabue, B.E. Watts, G. Bocelli, F. Calderón, G. Calestani, L. Righi, J. Mater. Sci. 39 (2004) 2107.
[22] B.G. Hyde, S. Andersson, Inorganic Crystal Structures, Wiley, New York, 1988.
[23] S. Denis, R. Dedryvère, E. Baudrin, S. Laruelle, M. Touboul, J. Olivier-Fourcade, J.C. Jumas, J.M. Tarascon, Chem. Mater. 12 (2000) 3733.
[24] E.J. Baran, I.L. Botto, Monatsh. Chem. 108 (1977) 311.
[25] J. Nilsson, A.R. Landa-Cánovas, S. Hansen, A. Andersson, J. Catal. 186 (1999) 442.
[26] E. Baba Ali, J.C. Bernède, A. Barreau, Mater. Chem. Phys. 63 (2000) 208.
[27] K. Asami, K. Hashimoto, Corros. Sci. 17 (1977) 559.
[28] S.L.T. Andersson, S. Järås, J. Catal. 64 (1980) 51.
[29] L. O'Mahony, T. Curtin, D. Zemlyanov, M. Mihov, B.K. Hodnett, J. Catal. 227 (2004) 270.
[30] J. Wong, F.W. Lytle, R.P. Messmer, D.H. Maylotte, Phys. Rev. B 30 (1984) 5596.
[31] M. Wakihara, Y. Shimizu, T. Katsura, J. Solid State Chem. 3 (1971) 478.
[32] D.B. Rogers, R.J. Arnott, A. Wold, J.B. Goodenough, J. Phys. Chem. Solids 24 (1963) 347.
[33] V. Nivoix, B. Gillot, Solid State Ionics 111 (1998) 17.
[34] B. Gillot, V. Nivoix, Mater. Res. Bull. 34 (1999) 1735.
[35] V. Nivoix, B. Gillot, Chem. Mater. 12 (2000) 2971.
[36] V. Nivoix, B. Gillot, Mater. Chem. Phys. 63 (2000) 24.
[37] B. Gillot, M. Nohair, Phys. Status Solidi A 176 (1999) 1047.
[38] M. Nohair, P. Perriat, B. Domenichini, B. Gillot, Thermochim. Acta 244 (1994) 223.
[39] R.D. Shannon, Acta Crystallogr. Sect. A 32 (1976) 751.
[40] C.-B. Wang, Y. Cai, I.E. Wachs, Langmuir 15 (1999) 1223.
[41] L.E. Briand, A.M. Hirt, I.E. Wachs, J. Catal. 202 (2001) 268.
[42] M. Bowker, R. Holroyd, M. House, R. Bracey, C. Bamroongwongdee, M. Shannon, A. Carley, Top. Catal. 48 (2008) 158.
[43] M.P. House, A.F. Carley, R. Echeverria-Valda, M. Bowker, J. Phys. Chem. C 112 (2008) 4333.
[44] C.J. Machiels, A.W. Sleight, J. Catal. 76 (1982) 238.
[45] L.J. Burcham, I.E. Wachs, Catal. Today 49 (1999) 467.
[46] L.E. Briand, W.E. Farneth, I.E. Wachs, Catal. Today 62 (2000) 219.
[47] X. Gao, I.E. Wachs, Top. Catal. 18 (2002) 243.
[48] B.M. Weckhuysen, D.E. Keller, Catal. Today 78 (2003) 25.
[49] M. Seman, J.N. Kondo, K. Domen, R. Radhakrishnan, S.T. Oyama, J. Phys. Chem. B 106 (2002) 12965.
[50] W.L. Holstein, C.J. Machiels, J. Catal. 162 (1996) 118.
[51] J. Döbler, M. Pritzsche, J. Sauer, J. Am. Chem. Soc. 127 (2005) 10861.
[52] A. Goodrow, A.T. Bell, J. Phys. Chem. C 111 (2007) 14753.
[53] F. Roozeboom, P.D. Cordingley, P.J. Gellings, J. Catal. 68 (1981) 464.
[54] G.D. Kolovertnov, G.K. Boreskov, V.A. Dzis'ko, B.I. Popov, D.V. Tarasova, G.G. Belugina, Kinet. Katal. (Engl. Transl.) 6 (1965) 1052.